Physica C: Superconductivity and its applications 575 (2020) 1353690

Contents lists available at ScienceDirect

Physica C: Superconductivity and its applications

journal homepage: www.elsevier.com/locate/physc

Optimized performance of an all-REBaCuO hybrid trapped field magnet lens (HTFML) with liquid nitrogen cooling

Sora Namba[a], Hiroyuki Fujishiro[a,*], Tatsuya Hirano[a], Tomoyuki Naito[a], Mark D Ainslie[b]

[a] Department of Physical Science and Materials Engineering, Faculty of Science and Engineering, Iwate University, 4-3-5 Ueda, Morioka 020-8551, Japan
[b] Department of Engineering, University of Cambridge, Trumpington Street, Cambridge CB2 1PZ, United Kingdom

ARTICLE INFO

Keywords:
REBaCuO bulk superconductor
Hybrid trapped field magnet lens (HTFML)
Magnetic shielding effect
Trapped field

ABSTRACT

The hybrid trapped field magnet lens (HTFML), proposed by the authors in 2018, is a promising device that is able to concentrate a magnetic field higher than the applied field continuously, even after removing the external applied field. In this study, we have investigated the optimized performance of the HTFML consisting of a GdBaCuO magnetic lens and a hollow, cylindrical EuBaCuO trapped field magnet (TFM) for various applied fields, B_{app}, at 77 K using liquid nitrogen. A maximum concentrated magnetic field of B_c = 1.83 T was obtained experimentally in the central bore of the HTFML for B_{app} = 1.80 T. For B_{app} higher than 1.80 T, the B_c value decreased, and was lower than the trapped field, B_t, in the single EuBaCuO TFM cylinder from field cooled magnetization. We have individually analyzed the electromagnetic behavior of the HTFML, single TFM hollow cylinder, and single magnetic lens during the magnetizing process using experimental and numerical simulation results. When the B_c value in the HTFML is lower than the B_t value of the single TFM cylinder for an identical B_{app}, the magnetic lens in the HTFML becomes partially magnetized, resulting in the generation of a negative magnetic field in the opposite direction. As a result, the concentrated field in the HTFML is reduced after the magnetizing process. The optimum applied field, B_{app}, which is the same magnitude as the maximum trapped field ability of the single TFM cylinder, provides the best performance. The maximum B_c value, and the B_{app} value that results in this B_c value, are determined by the critical current density, $J_c(B)$, characteristics of the bulk superconducting material used in the magnetic lens and TFM hollow cylinder in the HTFML.

1. Introduction

Higher magnetic fields are useful for various practical applications in a wide range of fields, including industry, engineering, medical science and fundamental physics. REBaCuO (RE = rare earth element or Y) bulk superconductors can be used as a compact, high-strength trapped field magnet (TFM) source due to the strong 'vortex pinning effect', which can produce magnetic fields over ten times higher than that of conventional permanent magnets. Trapped magnetic fields greater than 17 T have been reported by field cooled magnetization (FCM), e.g., 17.24 T at 29 K in a resin-impregnated YBaCuO bulk pair [1], 17.6 T at 26 K in a shrink-fit stainless steel-reinforced GdBaCuO bulk pair [2], and a recent record of 17.6 T at 22.5 K in composite GdBaCuO bulk stacks with stainless steel laminations [3]. A trapped field of 4.3 T has even been achieved in a GdBaCuO bulk pair even at 77 K [4].

Ring-shaped bulk superconductors, that can produce uniform and high magnetic fields in their central bore, are a powerful candidate for compact cryogen-free nuclear magnetic resonance (NMR) and magnetic resonance imaging (MRI) systems [5–7]. In addition, as a magnetic field concentrator, a magnetic lens made of bulk REBaCuO has been also developed [8–14]. When an external magnetic field is applied to the bulk magnetic lens in the superconducting state during the zero-field cooled magnetization (ZFCM) process, a shielding current is induced so as to prevent magnetic flux penetration into the bulk due to the so-called 'diamagnetic shielding effect'. Consequently, a magnetic field, B_c, is concentrated in the bore of the lens, which is higher than the applied field, B_{app}, generated from an external magnetizing coil.

The hybrid trapped field magnet lens (HTFML) was proposed by the authors in 2018 [15], which consists of a bulk TFM cylinder exploiting the 'vortex pinning effect', combined with a bulk magnetic lens exploiting the 'diamagnetic shielding effect'. Numerical simulations of the concept showed that the HTFML has potential to generate a magnetic field, B_c, higher than both the trapped field, B_t, in the single TFM cylinder by FCM and the external magnetizing field, B_{app}, even after the magnetization process, i.e., after removing the external field. Recently,

* Corresponding author.
E-mail address: fujishiro@iwate-u.ac.jp (H. Fujishiro).

https://doi.org/10.1016/j.physc.2020.1353690
Received 19 April 2020; Received in revised form 26 May 2020; Accepted 27 May 2020
Available online 29 May 2020
0921-4534/

we have demonstrated experimentally an HTFML comprised of a GdBaCuO magnetic lens and an MgB_2 TFM hollow cylinder on the cold stage of GM-cycle helium refrigerator, whereby a maximum B_c of 3.55 T was achieved at the central bore of the HTFML at T_s = 20 K after removing an applied field of B_{app} = 2.0 T [16].

An HTFML design that utilizes a REBaCuO TFM hollow cylinder with superior critical current density, $J_c(B, T)$, is expected not only to enhance the concentrated field, but also to broaden the range of practical applications, compared with using an MgB_2 TFM hollow cylinder, although additional challenges are presented in terms of cooling the device [15]. In a recent study, the basic performance of an HTFML consisting of an EuBaCuO TFM hollow cylinder of various heights and a GdBaCuO magnetic lens was investigated experimentally at 77 K using liquid nitrogen [17]. B_c = 0.80 T was achieved at the center of the HTFML for the tallest TFM cylinder after removing an applied magnetic field B_{app} = 0.50 T. Furthermore, these experimental results were reproduced well by numerical simulations. However, the relationships between the maximum B_c value in the HTFML, the B_t value in the single EuBaCuO TFM cylinder and the applied field, B_{app}, have not been clarified yet.

In this study, we investigate the performance of an HTFML consisting of only REBaCuO bulk superconductors (stacked EuBaCuO TFM hollow cylinders and a GdBaCuO magnetic lens) at 77 K for various B_{app} between 0.5 and 2.5 T at 77 K. In particular, we clarify the optimum applied field that results in the best performance of the HTFML, based on the both the experimental and simulation results.

2. Experimental procedure

2.1. Experimental setup of HTFML

Fig. 1(a) shows the cross-section of the experimental setup of the HTFML consisting of EuBaCuO hollow cylinders and a GdBaCuO magnetic lens. All of the bulks used in the experiments were fabricated by the QMG^{TM} method (Nippon Steel Corporation, Japan) [18]. Three hollow EuBaCuO cylinders (TFM-A, B and C) were stacked as the outer bulk TFM cylinder, which are referred to as "EuBaCuO TFM cylinder" or "TFM cylinder" in the paper. The dimensions of the EuBaCuO TFM cylinder are a 60 mm outer diameter (OD), 36 mm inner diameter (ID) and a height (H) of 54 mm. Each ring-shaped EuBaCuO bulk was reinforced by an Al alloy ring 5 mm in thickness (70 mm OD, 60 mm ID), which is a suitable material for the reinforcement of the bulk when applied to NMR apparatus because of its non-magnetic property and higher mechanical strength [6]. Fig. 1(b) shows the cross-section and top views of the "GdBaCuO magnetic lens" (or "magnetic lens"). The GdBaCuO magnetic lens was manufactured by Sarton Works Co. Ltd., Yokohama, Japan, two stacked GdBaCuO cylindrical bulks (OD = 36 mm, ID = 10 mm, H = 30 mm) into a cone-shape with OD = 30 mm, ID = 10 mm, ID2 = 26 mm, outer height (OH) = 30 mm and inner height (IH) = 8.0 mm. These dimensions were optimized using numerical simulations [19]. Two slits 200 μm in width were made to disrupt the circumferential flow of the shielding current, which plays an important role in magnetic flux concentration for the magnetic lens [8,15]. When an external magnetic field is applied to the GdBaCuO magnetic lens along the +z-direction, a shielding current flows counterclockwise around the central bore of the lens, as shown by the red arrows in Fig. 1(b). As a result, the magnetic field due to the shielding current is superimposed on the external applied field through the slits in the bore and the B_c value is enhanced.

The GdBaCuO magnetic lens was encapsulated in a stainless steel (SS) holder to prevent mechanical fracture due to a large Lorentz force generated during the magnetizing process. The SS holder and the Al alloy ring apply a compressive stress to the magnetic lens and the TFM cylinder, respectively, during the cooling process from room temperature to 77 K because of the difference in the thermal expansion coefficient with the ceramic bulk material. The magnetic field along the z-direction was measured at the center of the HTFML ($x = y = z = 0$ mm) using an axial-type Hall sensor (F W Bell, BHA-921). The external field, B_{ex}, was estimated from the current flowing through the magnetizing coil.

2.2. Magnetization procedure

Since the TFM cylinder and the magnetic lens are made of REBaCuO material with the same transition temperature, T_c = 92 K, individual temperature control is required to realize the HTFML effect. Fig. 2 shows the time sequence of the external magnetic field, B_{ex}, and the temperature, T, of the EuBaCuO TFM cylinder and GdBaCuO magnetic lens during the magnetizing procedure, which comprises the following five stages.

(1) An outer glass-fiber reinforced plastic (GFRP) container (96 mm in OD, 80 mm in ID), shown in Fig. 1(a) was placed in the room temperature bore (100 mm in diameter) of a cryocooled superconducting solenoid magnet (170 mm in OD, 120 mm in ID, 200 mm in H; JASTEC JMTD-10T100). The GdBaCuO magnetic lens encapsulated by the SS holder was placed in the inner GFRP container (35 mm in OD, 33 mm in ID), which was then placed in the outer GFRP container. Then, liquid nitrogen was poured into both GFRP containers (note that the TFM is not yet inserted).

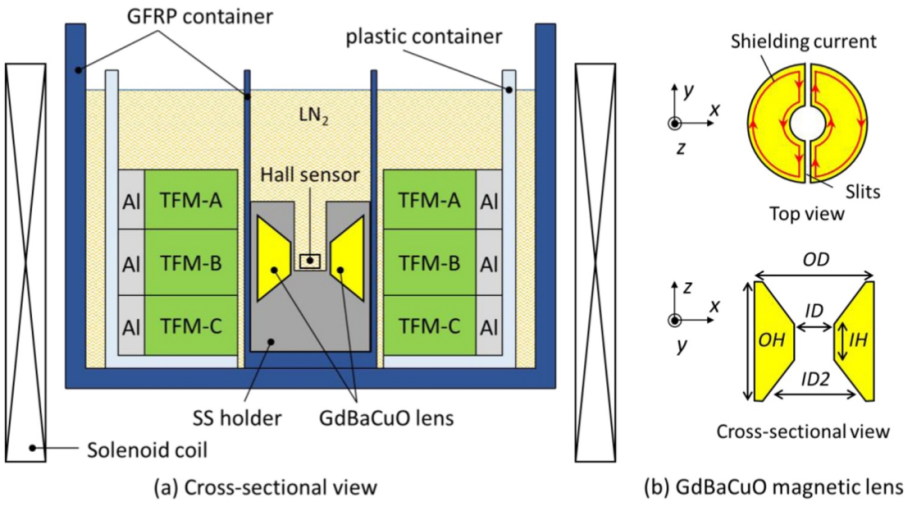

Fig. 1. (a) Cross-sectional view of the schematic illustration of the experimental setup for the HTFML immersed in liquid nitrogen [17], corresponding to the step (3) of the magnetizing process (see text). (b) Cross-sectional and top views of the GdBaCuO magnetic lens. When a magnetic field is applied along the +z-direction, the magnetic field penetrates from the slits and the shielding current also flows counterclockwise inside the lens as shown by the red arrows. As a result, the magnetic field is concentrated in the bore.

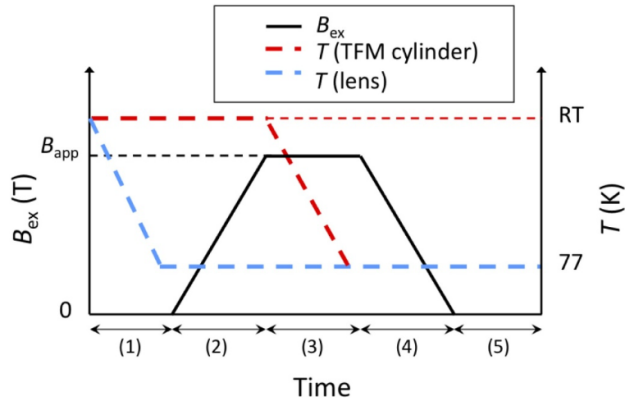

Fig. 2. Time dependence of the external field (black: left vertical axis), B_{ex}, at the center of the solenoid and the operating temperature (red: right vertical axis), T, during the magnetizing process to realize the HTFML [17]. The applied field, B_{app}, corresponds to the maximum B_{ex} value.

(2) The external magnetic field, B_{ex}, parallel to the $+z$-direction, was ramped up linearly to the maximum magnetic field of B_{app} (varying between 0.50 to 2.0 T) at a ramp rate of $+0.222$ Tmin^{-1}. During the ZFCM process, the magnetic field at the central position ($x = y = z = 0$ mm) of the HTFML is higher than B_{app} due to the shielding effect of the magnetic lens.
(3) After B_{ex} reached B_{app}, the EuBaCuO TFM cylinder in the plastic container was immersed slowly to the bottom of the outer GFRP container filled with liquid nitrogen. Thus, the EuBaCuO TFM cylinder was cooled down to 77 K under the magnetic field of B_{app}.
(4) After approximately 20 min later, B_{ex} was decreased linearly at -0.222 Tmin^{-1} down to zero. In this stage, the outer EuBaCuO TFM cylinder was magnetized by FCM and magnetic flux was trapped. A magnetic field at the center of the magnetic lens still remains due to the existence of the trapped field in the EuBaCuO TFM cylinder.
(5) As a result, the HTFML can reliably generate a magnetic field higher than the trapped field in the EuBaCuO TFM cylinder and B_{app}, even after $B_{ex} = 0$.

3. Numerical simulation framework

A three-dimensional numerical simulation model, including the magnetic lens, TFM cylinder and solenoid magnetizing coil, was constructed, based on the experimental setup shown in Fig. 1. In the model of the magnetic lens, two slits with 5° wide were used, which were wider than the experimental slits in order to reduce the calculation time related to finely meshing a narrower slit. The numerical simulation of the electromagnetic field was carried out using the commercial finite element method (FEM) software package, Photo-Eddy (Photon Ltd., Japan), which visualizes the magnetic field distribution in bulk superconductors, and helps us to understand the complex electromagnetic phenomena during the magnetization process. The nonlinear relationship between the electric field, E, and the current density, J, in the bulk superconductors is described by the power–n law, $E \propto J^n$ [20], where $n = 20$ as a typical value for HTS materials [21,22]. The bulks are assumed to be uniform without any imperfections or inhomogeneous superconducting characteristics.

Fig. 3 shows the assumed magnetic field dependence of the critical current density, $J_c(B)$, at 77 K of the bulks in the simulation, which is fitted using the following equation [23–26],

$$J_c(B) = J_{c1}\exp\left(-\frac{B}{B_L}\right) + J_{c2}\frac{B}{B_{max}}\exp\left[\frac{1}{k}\left(1-\left(\frac{B}{B_{max}}\right)^k\right)\right], \quad (1)$$

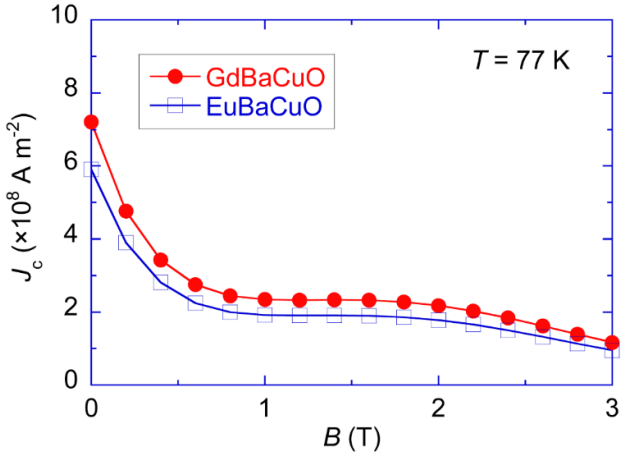

Fig. 3. $J_c(B)$ curves at 77 K for the EuBaCuO TFM cylinder and GdBaCuO magnetic lens used in the simulation.

Table 1
Fitting parameters of the $J_c(B)$ characteristics at 77 K for the EuBaCuO TFM cylinder and GdBaCuO magnetic lens, shown in Eq. (1).

	J_{c1} (A m^{-2})	B_L (T)	J_{c2} (A m^{-2})	B_{max} (T)	k
EuBaCuO TFM cylinder	5.9×10^8	0.4	1.8×10^9	1.7	2.4
GdBaCuO magnetic lens	7.2×10^8	0.4	2.2×10^9	1.7	2.4

where J_{c1} and J_{c2} are the magnitudes of the central and secondary peaks of $J_c(B)$, respectively, B_{max} is the secondary peak position, and B_L and k are coefficients. The fitting parameters for the EuBaCuO TFM cylinder and the GdBaCuO magnetic lens are given in Table 1 [17]. The values of J_{c1} and J_{c2} of the EuBaCuO TFM cylinder were determined in order to reproduce the experimental trapped field by FCM or ZFCM for the TFM-B, which consists of the EuBaCuO TFM cylinder [17]. The J_{c1} and J_{c2} values of the GdBaCuO magnetic lens were estimated to be slightly higher than those of the EuBaCuO TFM cylinder because of the fact that the trapped magnetic field of a QMG-GdBaCuO disk bulk with 60 mm in OD and 20 mm in H at 77 K was slightly higher than that of QMG-EuBaCuO disk bulk with the same size [27]. Isothermal conditions were assumed in the simulation, such that the temperature of the TFM cylinder and magnetic lens was set to a constant 300 K or 77 K during the magnetizing process, as shown in Fig. 2, because the ramp rate of $\pm$ 0.222 Tmin^{-1} was relatively slow.

4. Results and discussion

4.1. Single EuBaCuO TFM cylinder trapped field properties

Prior to the experiments on the HTFML, the single EuBaCuO TFM cylinder was magnetized by FCM to assess its trapped field capability. Fig. 4 shows the trapped field, B_t, at the center of the single EuBaCuO TFM cylinder, as a function of applied field, B_{app}, during FCM at 77 K. Here, the experimental B_t value was defined as the measured magnetic field at $t = 15$ min after the end of the ramp down of the magnetizing field. The B_t value was proportional to B_{app} between $B_{app} = 0.5$ and 2.0 T and was nearly the same as the corresponding B_{app}. For $B_{app} = 2.5$ T, $B_t = 1.86$ T was comparable to the maximum B_t of 1.90 T for $B_{app} = 2.0$ T. These results indicate that the EuBaCuO TFM cylinder was fully magnetized for $B_{app} \geq 2.0$ T at 77 K and the trapped field of $B_t \approx 1.9$ T was its maximum trapped field capability. In addition, the simulation results for the single TFM cylinder are also shown in Fig. 4 using the fitted $J_c(B)$ curve shown in Fig. 3. It can be seen that the simulation results of B_t reproduced the experimental ones

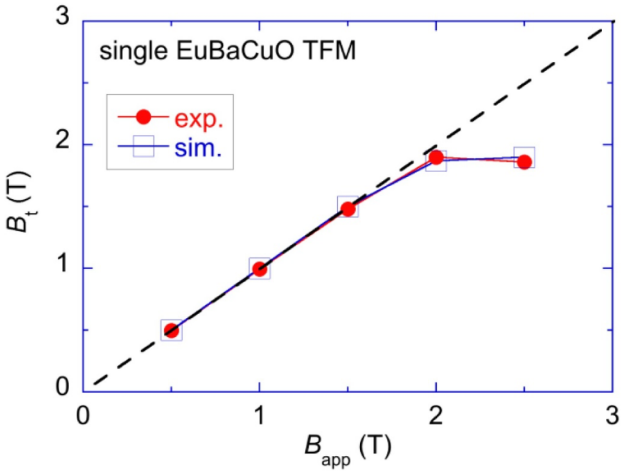

Fig. 4. Experimental and simulation results of the trapped fields, B_t, during FCM at 77 K at the center of the EuBaCuO TFM cylinder for various applied fields, B_{app}, from 0.5 to 2.5 T. B_t is defined as the measured magnetic field at t = 15 min after the end of the ramp down of the magnetizing field.

quantitatively. These results suggest that the trapped field properties of the single TFM cylinder could be estimated accurately using the fitted J_c (B) during FCM at 77 K.

4.2. GdBaCuO magnetic lens magnetic shielding properties

The magnetic shielding properties of the GdBaCuO magnetic lens were investigated during ZFCM and FCM operations at 77 K. For ZFCM operation, the external magnetic field increased and decreased for the magnetic lens at 77 K. On the other hand, for FCM operation, after the external field was stably applied to the magnetic lens at $T > T_c$, the lens was immersed in LN_2, and then the external field was ramped down to zero. Fig. 5(a) shows the time dependence of the concentrated magnetic field, $B_c^{ZFCM}(t)$, during ZFCM, and the trapped field, $B_t^{FCM}(t)$, during FCM for B_{app} = 2.0 T at the center of the lens. The time dependence of the external magnetic field, $B_{ex}(t)$, is also shown. In the ascending stage of the ZFCM process (increasing B_{ex} from 0 to 2.0 T), B_c^{ZFCM} exceeded the external field, B_{ex}, because of the magnetic field concentration due to the diamagnetic shielding effect. A maximum concentrated field of B_c^{max} = 2.30 T was achieved at $B_{ex} = B_{app}$ = 2.0 T for ZFCM. In the subsequent descending stage of the ZFCM process, the magnetic field gradually decreased and reached a negative value of $B_t^{ZFCM} = -0.394$ T at B_{ex} = 0 T, resulting from magnetic flux penetration and subsequent flux trapping in the lens [16]. This value was nearly the same as the trapped field of $B_t^{FCM} = -0.396$ T obtained by FCM, meaning that the total amount of the trapped magnetic flux in the lens for the ZFCM process is the same as that for the FCM process, as expected.

Fig. 5(b) shows experimental results of the maximum concentrated field, B_c^{max}(exp.), and final trapped field, B_t^{ZFCM}(exp.), at the center of the lens obtained by the ZFCM process, as a function of the applied field, B_{app}. The simulated B_c^{max}(sim.) obtained by ZFCM and the experimental results of B_t^{FCM}(exp.) obtained by FCM for B_{app} = 1.0 T and 2.0 T are also shown. The measured magnetic fields for $B_{ex} = B_{app}$ and t = 15 min after the ramp end are defined as B_c^{max}(exp.) and B_t(exp.), respectively. At the end of the ascending stage of the ZFCM process, *i.e.*, $B_{ex} = B_{app}$, the B_c^{max}(exp.) value was enhanced and increased linearly with increasing B_{app}, but the concentration ratio, B_c^{max}(exp.)/B_{app}, decreased gradually from 1.59 for B_{app} = 0.5 T to 1.09 for B_{app} = 2.5 T due to magnetic flux penetration into the magnetic lens. The B_c^{max}(sim.) value was slightly smaller than the B_c^{max}(exp.) value for higher B_{app}, which resulted from the tapered slits with 5° wide in the numerical model, compared with the actual slits 200 μm in width in experimental

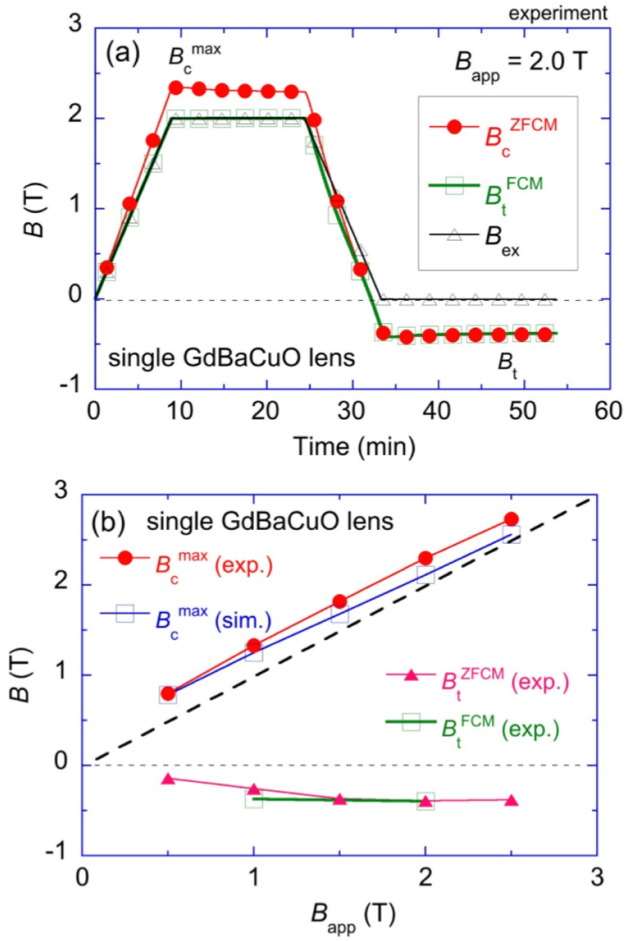

Fig. 5. (a) Time dependence of the concentrated magnetic field, $B_c^{ZFCM}(t)$, during ZFCM, and the trapped field, $B_t^{FCM}(t)$, during FCM for B_{app} = 2.0 T at the center of the GdBaCuO magnetic lens. The external magnetic field, $B_{ex}(t)$ is also shown. (b) The maximum concentrated field, B_c^{max}(exp.) and B_c^{max}(sim.), and final trapped field, B_t^{ZFCM}(exp.), obtained by the ZFCM process, and B_t^{FCM}(exp.) obtained by the FCM process, as a function of applied field, B_{app}.

lens structure. A negative trapped field, B_t^{ZFCM}(exp.), was obtained after the descending stage of the ZFCM, which increased with increasing applied field, since the more penetrated magnetic flux in the ascending stage was pinned in the magnetic lens. This negative B_t^{ZFCM}(exp.) value saturated for $B_{app} \geq$ 2.0 T, and nearly the same as B_t^{FCM}(exp.) ≈ -0.39 T for both B_{app} = 1.0 T and 2.0 T, suggesting that the magnetic lens was fully magnetized by ZFCM for $B_{app} \geq$ 1.5 T.

Fig. 6(a) shows the simulation results of the cross-sectional magnetic field profiles at z = 0 mm for the GdBaCuO magnetic lens, when B_{ex} reached B_{app} during the ZFCM process. The magnetic field outside of the lens ($x >$ 15 mm) is the same as the B_{app} generated from the magnetizing coil. For lower B_{app} = 0.5 T, a small amount of the flux penetration is observed into both outer and inner surfaces of the lens. At the same time, a perfectly shielded region (B = 0 T) exists in its central region (7 mm $\leq x \leq$ 12 mm). With the increase in the applied field, the amount of flux penetration into the lens increases and the perfectly shielded zone disappears for $B_{app} \geq$ 1.0 T. However, the magnetic field in the lens region (5 mm $\leq x \leq$ 15 mm) was slightly lower than the magnitude of the corresponding applied field in air by the shielding effect, which resulted in a slight magnetic field concentration in the bore of the lens. It should be noted that a faint shielding effect still remains even for higher B_{app} = 2.5 T in the magnetic lens region.

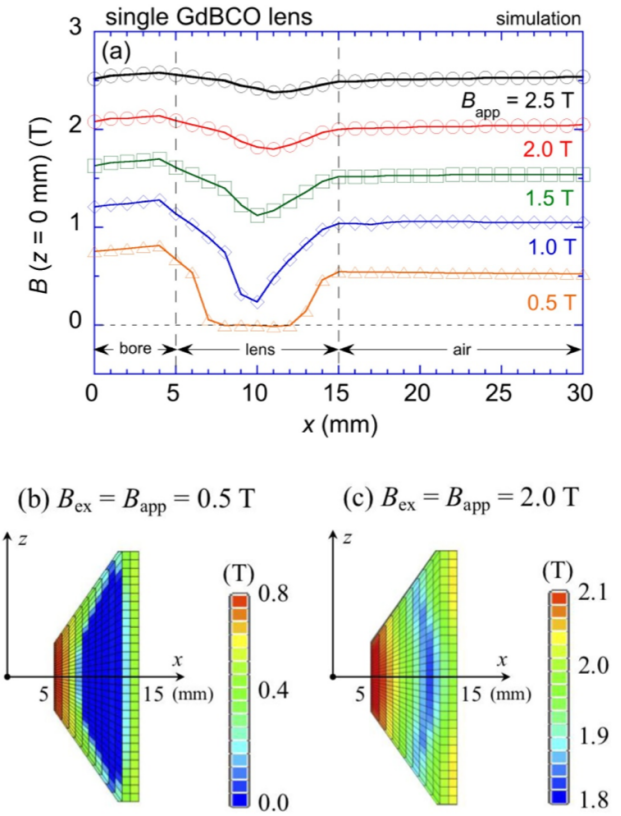

Fig. 6. (a) Simulation results showing the cross-sectional magnetic field profile at $z = 0$ mm for the GdBaCuO magnetic lens, when B_{ex} reached B_{app} during the ZFCM process. Magnetic field distribution within the lens for (b) $B_{ex} = B_{app} = 0.5$ T and (c) $B_{ex} = B_{app} = 2.0$ T during the ZFCM process.

Fig. 6(b) shows the magnetic field distribution for $B_{ex} = B_{app} = 0.5$ T, in which the presence of the perfectly shielded zone can be confirmed in the bore of the lens. The magnitude of the flux penetration at the inner lens surface was still larger than that at the outer lens surface because of the flux concentration in the center of the lens. Fig. 6(c) shows the magnetic field distribution in the lens at $B_{ex} = B_{app} = 2.0$ T during the ZFCM process. It is apparent that the magnetic flux penetration into the lens is much larger compared with Fig. 6(b). In addition, flux penetration into the tapered surfaces was confirmed, and the region of $B < 2.0$ T, which contributed to magnetic field concentration, can be also seen.

4.3. HTFML performance assessment

Fig. 7 shows the experimental results for the concentrated magnetic field, B_c, at the center of the HTFML after the magnetizing process, as a function of applied field, B_{app}. The experimental results for the trapped field, B_t, of the single EuBaCuO TFM cylinder by FCM are also shown for comparison, which are extracted from Fig. 4. For $B_{app} < 2.0$ T, the B_c value in the HTFML exceeded the B_t value in the single TFM cylinder, and a maximum concentrated field of $B_c = 1.83$ T was achieved for $B_{app} = 1.80$ T, which was slightly lower than the maximum trapped field of $B_t = 1.90$ T. The B_c value decreased to 1.60 T for $B_{app} = 2.5$ T, even though the B_t value scarcely changed. The simulation results of the B_c value are also shown in Fig. 7, which reproduced experimental ones well. These results suggest that the fitted $J_c(B)$ for each bulk material allows an accurate estimation of the HTFML performance.

Let us consider the fact that the B_c value for $B_{app} \geq 2.0$ T is lower than the B_t value. Fig. 8 shows experimental results of the time

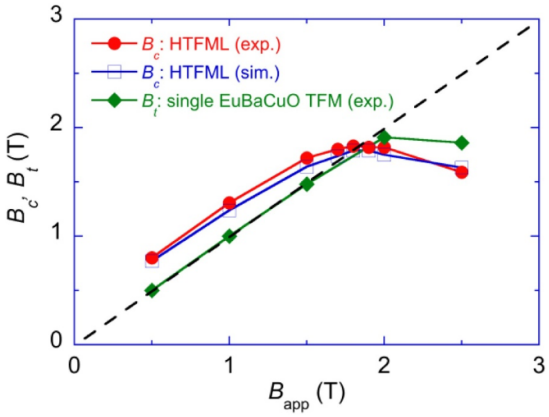

Fig. 7. Experimental and simulation results for the concentrated magnetic field, B_c, at the center of the HTFML after the magnetizing process for various applied fields, B_{app}. The experimental results for the trapped field, B_t, of the single EuBaCuO TFM cylinder by FCM are also shown for comparison.

dependence of $B_c(t)$ in the HTFML and $B_t(t)$ in the single EuBaCuO TFM cylinder during the descending stage from $B_{app} = 1.0$, 2.0 and 2.5 T. The beginning of the decrease in B_{ex} from B_{app} is defined as $t = 0$. In the case of the HTFML, the magnetic field was applied from the magnetizing coil in the ascending stage. However, during the descending stage ($t > 0$) of FCM for the EuBaCuO TFM cylinder, the magnetic field source gradually shifted from the magnetizing coil to the magnetized EuBaCuO TFM cylinder. This means that the final B_c value in the HTFML is generated from the trapped field of the EuBaCuO TFM cylinder. Since the magnetic field generated from the magnetizing coil was concentrated by the lens in the ascending stage, B_c at $t = 0$ in the HTFML was higher than $B_{ex} = B_{app}$ and was equal to B_c^{max} obtained by the single GdBaCuO magnetic lens shown in Fig. 5(b). For $B_{app} = 1.0$ T, as shown in Fig. 8(a), a constant field of $B_c = 1.3$ T was continuously generated in the HTFML with increasing time because the magnetic field of $B_t = 1.0$ T was trapped in the EuBaCuO TFM cylinder. On the other hand, for $B_{app} = 2.0$ T as shown in Fig. 8(b), $B_c(t)$ starts to fall at the end of the descending stage ($t \sim 9$ min), at which a slight decrease in $B_t(t)$ of the TFM cylinder was also observed mainly due to flux creep at the same time, and $B_c(t)$ eventually became lower than $B_t(t)$ of the TFM cylinder at $t = 15$ min. For higher $B_{app} = 2.5$ T as shown in Fig. 8(c), $B_c(t)$ in the HTFML decreased largely due to the decrease in $B_t(t)$ of the TFM cylinder as well.

Figu. 9(a) and (b), respectively, show the simulation results of the cross-sectional magnetic field profiles for the HTFML ($z = 0$ mm) at the beginning of the descending stage, $B(t = 0)$, and those after 15 min from the end of the descending stage, $B(t = t_{end})$, for various applied fields, B_{app}. At $t = 0$, as shown in Fig. 9(a), the magnitude of magnetic field in the TFM cylinder (20 mm $\leq x \leq$ 30 mm) was equal to the externally applied magnetic field, B_{app}. After the descending stage, as shown in Fig. 9(b), at which the external field was reduced to zero, a circumferential superconducting current was induced in the TFM cylinder and then the TFM cylinder was magnetized. For $B_{app} \geq 2.0$ T, that is enough to fully magnetize the present TFM cylinder at 77 K – similar trapped field profiles were observed in the TFM cylinder (20 mm $\leq x \leq$ 30 mm). In the magnetic lens region (5 mm $\leq x \leq$ 15 mm), the $B(t = 0)$ profile for $B_{app} \leq 2.0$ T is nearly the same as the B ($t = t_{end}$) profile. On the other hand, for higher $B_{app} = 2.5$ T, there was a significant difference between $B(t = 0)$ and $B(t = t_{end})$ profiles; the magnetic flux was trapped in the magnetic lens after the descending stage.

Fig. 9(c) shows the difference in the magnetic field profile, ΔB (i.e., $B(t = 0) - B(t = t_{end})$), at $z = 0$ mm, between before and after the descending stage for various applied fields. In the TFM cylinder region

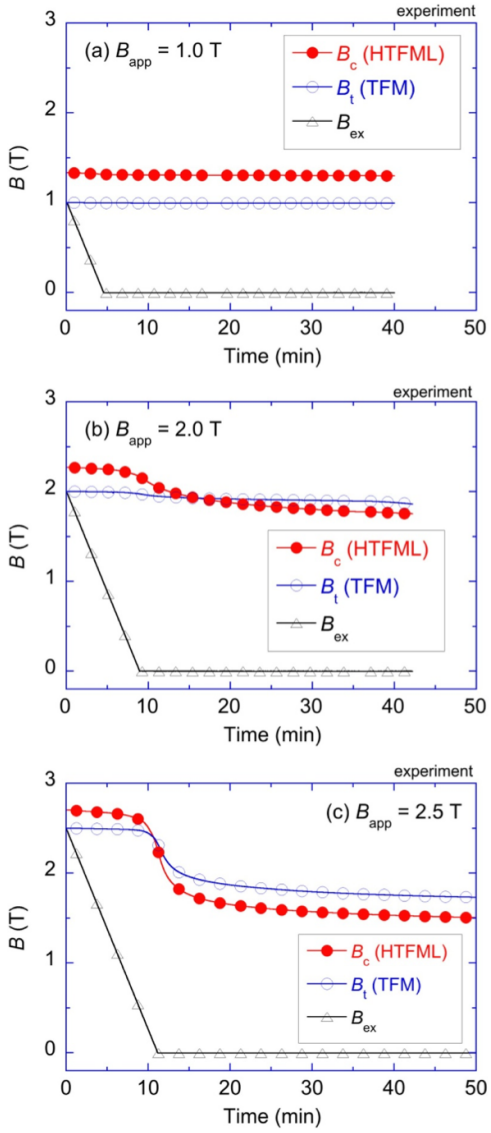

Fig. 8. Time dependence of the concentrated field, $B_c(t)$, at the center of the HTFML and the trapped field, $B_t(t)$, of the single EuBaCuO TFM cylinder during the descending stage of the magnetizing process for (a) B_{app} = 1.0 T, (b) 2.0 T, and (c) 2.5 T. The beginning of the decrease in B_{ex} from B_{app} is defined as t = 0.

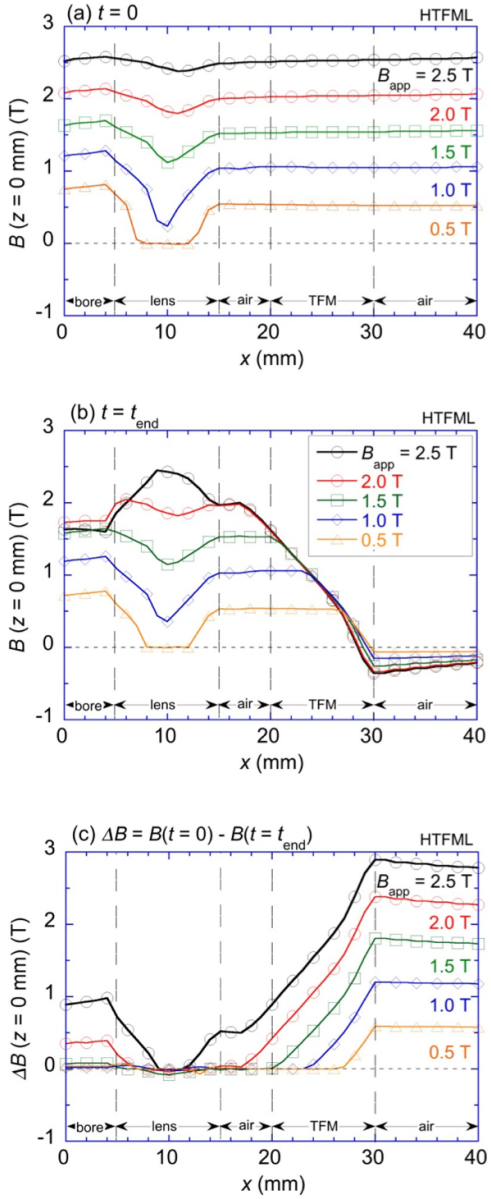

Fig. 9. Numerical simulation results of the cross-sectional magnetic field profiles for various applied fields at z = 0 mm for the HTFML: (a) at the beginning of the descending stage, $B(t$ = 0), and (b) t = 15 min after the end of the descending stage, $B(t$ = $t_{end})$. (c) Difference in the magnetic field profile, ΔB = $B(t$ = 0) − $B(t$ = $t_{end})$, at z = 0 mm between before and after the descending stage.

(20 ≤ x ≤ 30 mm), a positive ΔB value means the "extra magnetic field" that was escaped from the TFM without being trapped during the descending process. The ΔB value increased with increasing B_{app} and the TFM cylinder trapped the same magnetic field as B_{app}. In contrast, the positive ΔB in the magnetic lens region (5 ≤ x ≤ 15 mm) means to be "magnetized" or "flux trapped", which was almost zero for B_{app} ≤ 2.0 T, meaning that the magnetic field in the magnetic lens did not change before and after the descending stage. A slight positive ΔB region was observed only at the inner region of the lens (5 ≤ x ≤ 7 mm) for B_{app} = 2.0 T. On the other hand, a large positive ΔB region existed at the inner and outer lens regions for B_{app} = 2.5 T, which indicates that the magnetic lens was magnetized partially for the applied magnetic field, B_{app}, higher than the maximum B_t of the TFM cylinder. As a result, the trapped magnetic flux in the magnetic lens created a negative magnetic field (i.e., along the –z-direction), which was the cause of the deterioration of the HTFML effect. We conclude that an applied field, B_{app}, of the same magnitude as the maximum trapped field capability of the TFM cylinder (i.e., B_t = 1.9 T) results in the best HTFML performance. In the present HTFML, consisting of only REBaCuO bulks at 77 K, a maximum concentrated field of B_c = 1.83 T was achieved in the HTFML after the magnetizing process with B_{app} = 1.80 T, which was almost the same as the maximum trapped field, B_t, of the single EuBaCuO TFM cylinder.

In previous work by the authors, we presented experimental results for an HTFML comprised of a GdBaCuO magnetic lens and an MgB_2 TFM hollow cylinder at T_s = 20 K [16]. Fig. 10(a) summarizes these experimental results, as a function of B_{app}, extracted from [16]. The B_t value for the single MgB_2 TFM, and B_c^{max} and B_t^{FCM} values for the single GdBaCuO lens are also shown. The concentrated magnetic field was B_c = 1.99 T at B_{app} = 1.0 T, took a maximum value of B_c = 3.55 T for

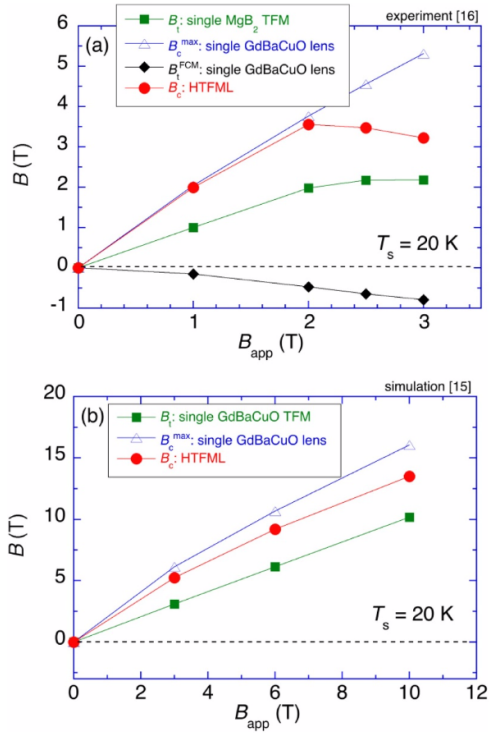

Fig. 10. (a) A summary of the experimental results for the HTFML comprised of a GdBaCuO magnetic lens and an MgB_2 TFM hollow cylinder at T_s = 20 K, extracted from [16]. (b) Numerical simulation results for the HTFML comprised of GdBaCuO magnetic lens and GdBaCuO TFM hollow cylinder at T_s = 20 K, extracted from [15].

B_{app} = 2.0 T, and then decreased to B_c = 3.22 T for a higher applied field of B_{app} = 3.0 T. An optimum B_{app} = 2.0 T required to maximize the B_c value for the HTFML existed, around which the B_t^{FCM} value took a maximum value of 2.18 T. These B_{app} dependencies at T_s = 20 K are quite similar to those for the present results shown in Figs. 5(b) and 7 at T_s = 77 K. This present study qualitatively supports these previous results.

We now present similar relationships for the HTFML comprised of only GdBaCuO bulks. Fig. 10(b) shows the numerical simulation results for the B_c value for the HTFML comprised of a GdBaCuO magnetic lens and GdBaCuO TFM hollow cylinder at T_s = 20 K, as a function of B_{app}, extracted from [15]. The concentrated magnetic field, B_c, monotonously increased with increasing B_{app}, and B_c = 13.49 T was achieved for B_{app} = 10 T. The B_t value for the single GdBaCuO TFM during FCM, and B_c^{max} value for the single GdBaCuO lens are also shown, which also increased monotonously with increasing B_{app}. The relationships between these parameters (B_c, B_c^{max} and B_t) are similar to the cases shown in Fig. 10(a); that is, B_c is enhanced compared with B_t, and is smaller than B_c^{max} for each B_{app}. These results indicate that the maximum B_c value could be enhanced for an all-REBaCuO HTFML magnetized at an operating temperature lower than 77 K. However, in the all-REBaCuO HTFML at 20 K, there was no B_{app} value that resulted in a B_c peak for applied fields up to 10 T. This result strongly suggests that the B_t value in the GdBaCuO TFM cylinder was not saturated and that an optimum B_{app} should exist for B_{app} values higher than 10 T for the HTFML comprised of higher $J_c(B)$ REBaCuO bulks and/or at lower T_s operation. In this case, the optimum B_{app}, which is of the same magnitude as the maximum trapped field capability of the single GdBaCuO TFM cylinder, provides the best performance of the HTFML. The relationships between the maximum B_c value in the HTFML, the B_t value in the single TFM cylinder and the optimum B_{app} value are determined depending on the $J_c(B, T)$ characteristics of the bulk superconductors comprising the magnetic lens and TFM hollow cylinder in the HTFML device. The HTFML comprised of all REBaCuO bulks with higher $J_c(B)$ at lower T_s operation is necessary to achieve higher performance of HTFML effect.

5. Conclusion

We have investigated experimentally and numerically the performance of an all-REBaCuO hybrid trapped field magnet lens (HTFML), which consists of an EuBaCuO TFM hollow cylinder and a GdBaCuO magnetic lens, at 77 K using liquid nitrogen. The important results and conclusions of this study are summarized as follows.

(1) A maximum concentrated magnetic field of B_c = 1.83 T was obtained experimentally at the center of the HTFML for B_{app} = 1.80 T. For B_{app} higher than 1.80 T, the B_c value decreased, which was lower than the trapped field, B_t, in the single EuBaCuO TFM cylinder by FCM.
(2) The numerical simulation results well reproduced the experimental results of the magnetic field amplification performance of the HTFML, as well as the performance of the single TFM cylinder and single magnetic lens individually. These results suggest that the $J_c(B)$ characteristics of the EuBaCuO TFM cylinder determined by FCM and of the GdBaCuO magnetic lens determined by ZFCM can precisely estimate the experimental results.
(3) The numerical simulations revealed that the magnetic lens in HTFML was magnetized partially after the magnetization process for B_{app} values higher than the maximum B_t of the TFM cylinder, resulting in the generation of a negative magnetic field in the opposite direction. The optimum B_{app}, which is the same magnitude as the maximum trapped field capability of the single TFM cylinder, results in the best performance of the HTFML. The relationships between the maximum B_c value of the HTFML, the B_t value of the single TFM cylinder and the optimum B_{app} value can be determined and depend on the $J_c(B, T)$ characteristics of the bulk superconductors comprising the magnetic lens and TFM hollow cylinder in the HTFML device.

Declaration of Competing Interest

The authors declare that they have no known competing financial interests or personal relationships that could have appeared to influence the work reported in this paper.

Acknowledgement

The authors thank Mr K. Takahashi of Iwate University for the valuable discussion and suggestion, and Mr Y. Yanagi of IMRA Material R&D Co., Ltd, Japan, for his experimental supports. This research was supported by Adaptable and Seamless Technology transfer Program through Target-driven R&D (A-STEP) from Japan Science and Technology Agency (JST), Grant No. VP30218088419 and by JSPS KAKENHI Grant No. 19K05240. M. D. Ainslie would like to acknowledge financial support from an Engineering and Physical Sciences Research Council (EPSRC) Early Career Fellowship, EP/P020313/1. All data are provided in full in the results section of this paper.

References

[1] M. Tomita, M. Murakami, High-temperature superconductor bulk magnets that can trap magnetic fields of over 17 tesla at 29 K, Nature 421 (2003) 517–520.
[2] J.H. Durrell, A.R. Dennis, J. Jaroszynski, M.D. Ainslie, K.G.B. Palmer, Y.-H. Shi, A.M. Campbell, J. Hull, M. Strasik, E.E. Hellstrom, D.A. Cardwel, A trapped field of 17.6 T in melt-processed, bulk Gd-Ba-Cu-O reinforced with shrink-fit steel, Supercond. Sci. Technol. 27 (2014) 082001.
[3] K.Y. Huang, Y.-H. Shi, J. Srpčič, M.D. Ainslie, D.K. Namburi, A.R. Dennis, D. Zhou,

M. Boll, M. Filipenko, J. Jaroszynski, E.E. Hellstrom, D.A. Cardwell, J.H. Durrell, Composite stacks for reliable >17 T trapped fields in bulk superconductor magnets, Superconnd. Sci. Technol. 33 (2020) 02LT01.
[4] S. Nariki, N. Sakai, M. Murakami, Melt-processed Gd–Ba–Cu–O superconductor with trapped field of 3 T at 77 K, Supercond. Sci. Technol. 18 (2005) S126–S130.
[5] T. Nakamura, Y. Itoh, M. Yoshikawa, T. Oka, J. Uzawa, Development of a superconducting magnet for nuclear magnetic resonance using bulk high-temperature superconducting materials, Concepts Magn. Reson. B 31B (2007) 65–70.
[6] T. Nakamura, D. Tamada, Y. Yanagi, Y. Itoh, T. Nemoto, H. Utumi, K. Kose, Development of a superconducting bulk magnet for NMR and MRI, J. Magn. Reson. 259 (2015) 68–75.
[7] K. Ogawa, T. Nakamura, Y. Terada, K. Kose, T. Haishi, Development of a magnetic resonance microscope using a high T_c bulk superconducting magnet, 2011, Appl. Phys. Lett. 98 (2011) 234101.
[8] Z.Y. Zhang, S. Matsumoto, R. Teranishi, T. Kiyoshi, Magnetic field, temperature and mechanical crack performance of a GdBCO magnetic lens, Supercond. Sci. Technol. 25 (2012) 115012.
[9] S. Choi, J.-H. Yoon, B.-S. Lee, M.-S. Won, J.-W. Ok, Z.-Y. Zhang, T. Kiyoshi, S. Matsumoto, S.-H. Lee, Magnetic lens effect using Gd-Ba-Cu-O bulk superconductor in very high magnetic field, J. Appl. Phys. 111 (2012) 07E728.
[10] T. Kiyoshi, S. Choi, S. Matsumoto, T. Asano, D. Uglietti, Magnetic Flux Concentrator Using Gd-Ba-Cu-O Bulk Superconductors, IEEE Trans. Appl. Supercond. 19 (2009) 2174–2177.
[11] Z.Y. Zhang, S. Matsumoto, R. Teranishi, T. Kiyoshi, Improving the properties of GdBCO magnetic lenses by adopting a new design and resin impregnation, Supercond. Sci. Technol. 26 (2013) 045001.
[12] T. Asano, K. Itoh, S. Matsumoto, T. Kiyoshi, H. Wada, G. Kido, Enhanced concentration of the magnetic flux in a superconducting cylinder, IEEE Trans. Appl. Supercond. 15 (2005) 3157–3160.
[13] S. Choi, T. Kiyoshi, S. Matsumoto, Magnetic field amplifier employing high-T_c bulk superconductor, J. Appl. Phys. 105 (2009) 07E705.
[14] A. Miyazoe, R. Nakagawa, C. Hori, H. Tanaka, Y. Imamura, Temporal stabilization of magnetic flux focused by superconducting magnetic lens, IEEE Trans. Appl. Supercond. 28 (2018) 4700205.
[15] K. Takahashi, H. Fujishiro, M.D. Ainslie, A new concept of a hybrid trapped field magnet lens, Supercond. Sci. Technol. 31 (2018) 044005.
[16] S. Namba, H. Fujishiro, T. Naito, M.D. Ainslie, K. Takahashi, Experimental realization of a hybrid trapped field magnet lens using a GdBaCuO magnetic lens and MgB_2 bulk cylinder, Supercond. Sci. Technol. 32 (2019) 12LT03.
[17] S. Namba, H. Fujishiro, T. Naito, M.D. Ainslie, D. Zhou, Realisation of hybrid trapped field magnetic lens (HTFML) consisting of REBCO bulk lens and REBCO bulk cylinder at 77 K, J. Phys. Conf. Series (2020) at press.
[18] M. Morita, M. Sawamura, S. Takebayashi, K. Kimura, H. Teshima, M. Tanaka, K. Miyamoto, M. Hashimoto, Processing and properties of QMG materials, Physica C 235–240 (1994) 209–212.
[19] S. Namba, H. Fujishiro, M.D. Ainslie, K. Takahashi, T. Naito, D.K. Namburi, D. Zhou, Design optimization of a hybrid trapped field magnet lens (HTFML), IEEE Trans. Appl. Supercond. 29 (2019) 6801605.
[20] J. Rhyner, Magnetic properties and AC-losses of superconductors with power law current—voltage characteristics, Physica C 212 (1993) 292–300.
[21] D.M. Sheen, S.M. Ali, M.D. Abouzahra, J.A. Kong, Application of the three-dimensional finite-difference time-domain method to the analysis of planar microstrip circuits, IEEE Trans. Magn. 38 (2002) 849–852.
[22] M.D. Ainslie, H. Fujishiro, Modelling of bulk superconductor magnetization, Supercond. Sci. Technol. 28 (2015) 053002.
[23] M. Jirsa, L. Půst, D. Dlouhý, M.R. Koblischka, Fishtail shape in the magnetic hysteresis loop for superconductors: interplay between different pinning mechanisms, Phys. Rev. B 55 (1997) 3276–3284.
[24] M. Jirsa, M. Muralidhar, M. Murakami, K. Noto, T. Nishizaki, N. Kobayashi, Jc-B performance study of an OCMG (Nd-Eu-Gd)-123 material doped by sub-micrometre Gd-211 particles, Supercond. Sci. Technol. 14 (2001) 50–57.
[25] M. Muralidhar, N. Sakai, M. Jirsa, N. Koshizuka, M. Murakami, Direct observation and analysis of nanoscale precipitates in (Sm, Eu, Gd)$Ba_2Cu_3O_y$, Appl. Phys. Lett. 85 (2004) 3504.
[26] T. Kii, R. Kinjo, N. Kimura, M. Shibata, M.A. Bakr, Y.W. Choi, M. Omer, K. Yoshida, K. Ishida, T. Komai, K. Shimahashi, T. Sonobe, H. Zen, K. Masuda, H. Ohgaki, Low-temperature operation of a bulk HTSC staggered array undulator, IEEE Trans. Appl. Supercond. 22 (2012) 4100904.
[27] S. Nariki, H. Teshima, M Morita, Performance and applications of quench melt-growth bulk magnets, Supercond. Sci. Technol. 29 (2016) 034002.